

Chromatic aberration correction: an enhancement to the calibration of low-cost digital dermoscopes

Paul Wighton^{1,2,3}, Tim K. Lee^{1,2,3}, Harvey Lui^{2,3}, David McLean³ and M. Stella Atkins¹

¹School of Computing Science, Simon Fraser University, Burnaby, BC, Canada, ²Cancer Control Research and Cancer Imaging, BC Cancer Agency, Vancouver, BC, Canada and ³Department of Dermatology and Skin Science, Photomedicine Institute, University of British Columbia and Vancouver Coastal Health Research Institute, Vancouver, BC, Canada

Background/purpose: We present a method for calibrating low-cost digital dermoscopes that corrects for color and inconsistent lighting and also corrects for chromatic aberration. Chromatic aberration is a form of radial distortion that often occurs in inexpensive digital dermoscopes and creates red and blue halo-like effects on edges. Being radial in nature, distortions due to chromatic aberration are not constant across the image, but rather vary in both magnitude and direction. As a result, distortions are not only visually distracting but could also mislead automated characterization techniques.

Methods: Two low-cost dermoscopes, based on different consumer-grade cameras, were tested. Color is corrected by imaging a reference and applying singular value decomposition to determine the transformation required to ensure accurate color reproduction. Lighting is corrected by ima-

ging a uniform surface and creating lighting correction maps. Chromatic aberration is corrected using a second-order radial distortion model.

Results: Our results for color and lighting calibration are consistent with previously published results, while distortions due to chromatic aberration can be reduced by 42–47% in the two systems considered.

Conclusion: The disadvantages of inexpensive dermoscopy can be quickly substantially mitigated with a suitable calibration procedure.

Key words: digital dermoscopy – calibration – chromatic aberration – color and lighting correction

© 2011 John Wiley & Sons A/S

Accepted for publication 10 December 2010

WE PRESENT a method to calibrate inexpensive digital dermoscopes, made by attaching a traditional dermoscope to a consumer-grade digital camera. Such 'low-cost' digital dermoscopes are becoming increasingly popular as the prevalence of dermoscopic use in the clinic increases, and the cost of digital cameras decreases. It is hoped that such systems will lead to increased patient care through the use of teledermatology (1) or automated diagnostic methods (2) as well as enable the generation of a large database of various skin conditions to facilitate future research.

The nature of such digital dermoscopes poses several challenges. Firstly, the illumination across the field of view is not consistent, resulting in separate areas of over- and under-exposure within the same image. Secondly, the color of the image acquired is not accurate. Commercial digital cameras are optimized to operate under certain typical lighting conditions (such as sunlight, incandescent light, etc.), and thus have

difficulty estimating the properties of unconventional light sources such as those within dermoscopes. Moreover, consumer-grade cameras are more concerned with presenting visually esthetic images, rather than a faithful rendition of color *per se*.

These issues have been identified in the past, and calibration methods to render accurate color and to correct inconsistent lighting have been proposed (3–6). These methods acquire images of reference colors, which are used to derive transformations for accurate color reproduction as well as 'intensity maps' to correct for variations in lighting intensity.

In this paper, in addition to calibrating for color and lighting, we examine a distortion effect known as chromatic aberration, and correct for it accordingly. Chromatic aberration occurs when the refractive index of the optics is not constant with respect to wavelength. This effect is illustrated in Fig. 1. As the refractive index of the lens varies slightly with wavelength, the color of

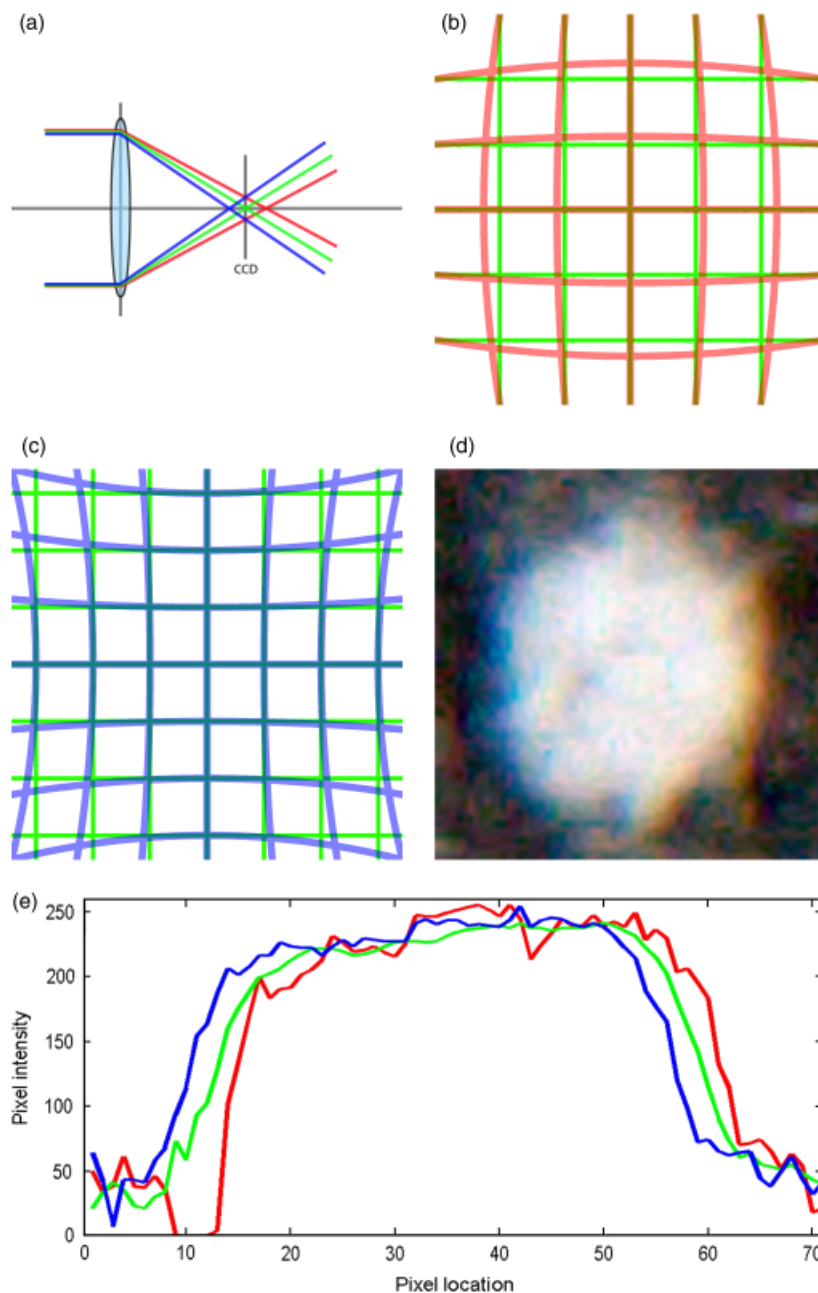


Fig. 1. Chromatic aberration (a) occurs when the refractive index of light varies with respect to wavelength. Relative to the green channel, this results in a (b) 'barrel' distortion of the red channel and a (c) 'pincushion' distortion of the blue. These distortions cause edges to appear in slightly different locations in each color channel, resulting in (d) blue and red 'halo' effects. Plotting the pixel intensities across a section of the square (e), it is evident that the location of the edges varies with respect to the color channel.

the light will affect the location of the focal plane. If the camera is set such that the green light is in focus, the red light will resolve slightly behind the focal plane while the blue light will resolve slightly in front. The result, relative to the green channel, is a 'barrel' distortion of the red channel and a 'pincushion' distortion of the blue channel. Expensive digital skin imaging systems can correct this optically; however, digital dermoscopy seems to be trending toward mating an already available dermoscope with an inexpensive digital

camera in the name of cost and convenience. While distortions due to chromatic aberration can be partially alleviated by decreasing the camera aperture size (thereby restricting the use of the lens to the center, where the distortion effects are minimized), such distortions are still evident when using inexpensive components. Being radial in nature, distortions due to chromatic aberration are not constant across the image, but rather vary in both magnitude and direction. Such distortions are visually distracting

and possibly clinically confounding. Furthermore, these distortions could also mislead automated characterization techniques (such as the automated identification of occluding hair or dermoscopic structures). For example, the variance of color within a lesion is an extremely important feature in both clinical as well as automated diagnosis (2), the accuracy of which would certainly be curbed by the introduction of spurious shades of red and blue. As a result, a software-based method of chromatic aberration correction is becoming increasingly necessary. We present a calibration method that not only corrects for inconsistent lighting and ensures accurate color reproduction but also corrects for chromatic aberration.

Methods

The imaging systems

We use two digital dermoscope systems in order to design and validate our calibration method. The first is a Dermlite II Pro (3Gen LLC, San Juan Capistrano, CA, USA) attached to a Canon Powershot G9 (Canon Inc., Tokyo, Japan) digital camera using a custom lens adapter (Lensmate, Gig Harbor, WA, USA) and standard stepping rings. A custom light shroud was machined and attached to the end of the dermoscope so that no ambient lighting would be present in the images. Images are acquired in the ‘raw’ mode with a resolution of 4000×3000 pixels. The spatial resolution is approximately 0.0073 mm^2 . The second system is a Dermlite II Pro attached to a Sony Cybershot DSC-W300 (Sony Corporation, Tokyo, Japan) using a custom lens adapter. The Sony camera acquires jpeg images with a resolution of 4224×3168 pixels and an approximate spatial resolution of 0.0063 mm^2 . We refer to these systems as the ‘Canon system’ and the ‘Sony system,’ respectively. As the magnitude of chromatic aberration is related to the aperture size of the camera, both cameras were set to use the smallest possible aperture size. The Canon camera parameters were set to: iso 100, shutter 1/30, f/5.0 and the Sony camera parameters were set to: iso 100, shutter 1/40, f/5.6.

A 24-patch color chart (X-Rite, Grand Rapids, MI, USA) and a black and white checkered pattern are used to calibrate the system. The freely available, open-source tool ddraw (7) is used to process the raw sensor data and convert it to uncalibrated CIE XYZ colorspace (8). An

S2000 spectrometer (Ocean Optics, Dunedin, FL, USA) was used to measure the reflectance curve of each color patch of the color chart, which acts as the ground truth color measurement.

A note on colorspace

Three colorspace are used throughout this paper. The first is CIE XYZ, which, when properly calibrated, is linear with respect to the sensitivities of the retinal cone cells in a standard human observer. When uncalibrated (as is when ddraw is used to convert from ‘raw’ format), it is linear with respect to the sensitivities of the camera’s CCD. Both color and lighting corrections are performed in this space. The second colorspace used is sRGB, which is a standardized colorspace used for display under typical viewing conditions. It is non-linear with respect to CIE XYZ because of the inclusion of a ‘gamma correction’ step, which compensates for the non-linearities of display devices. Because gamma correction is implicit in sRGB, we do not perform an explicit gamma correction step as in (4). Chromatic aberration is performed in this space and all images throughout this paper are presented in sRGB. The third colorspace used is CIE $L^*a^*b^*$, which is an approximately perceptually uniform colorspace, but non-linear with respect to both XYZ and sRGB. This colorspace is used to compare our method with previous results (3). Conversions between these three colorspace are well defined (8).

Color calibration

Given a color $c = [x \ y \ z]^T$ in the camera’s uncalibrated CIE XYZ colorspace, we transform it into the calibrated colorspace $c^* = [x^* \ y^* \ z^*]^T$ via a 3×3 color transformation matrix, M :

$$c^* = Mc$$

To compute M , we measure each of the 24 patches of the color chart using the dermoscope as well as the spectrometer. An image of each color patch is acquired using the dermoscope and is converted to an uncalibrated CIE XYZ space. The color of each patch is calculated by averaging over a small area in the center of the image where the lighting is the strongest. These uncalibrated color values are stored in a 24×3 matrix C . Next, the spectral reflectance curves of each of the 24 color patches are measured using a spectrometer. These reflectance curves are then multiplied by the three CIE standard observer matching

functions (8), which approximate the absorption spectra of the short, medium and long cones of the human retina, respectively. The resulting spectra are then integrated, yielding a point in the CIE XYZ space. These calibrated color values are stored in a 24×3 matrix C^* . It then follows that

$$C^* = MC$$

and the least squares solution for M is obtained via singular value decomposition

$$M = (C^T C)^{-1} C^T C^*$$

Once the transformation matrix M is computed, acquired images are transformed to the CIE XYZ space by multiplying uncalibrated color values by M . An example of this is shown in Fig. 2.

Lighting calibration

After calibrating for color, the colors in the center of the images are now much more accurate; however, the intensity of the lighting is not consistent across the image and must therefore be accounted for. We correct for this inconsistency by creating an illumination correction map (4).

To create this map, we consider the white patch on the color chart. Gaussian blurring is applied to the acquired image of this patch to remove any high-frequency variations (such as imperfections in the surface, dust, etc.) and the result for each channel is stored in the matrix X_W , Y_W and Z_W , respectively. We then relate these acquired values to the ground truth values obtained using the spectrometer data (X_S , Y_S , Z_S). The correction map for the X channel (X_C) is then computed as follows:

$$X_C = \frac{X_S}{X_W}$$

Y_C and Z_C are similarly computed. Newly acquired images are then corrected by pairwise multiplication with this correction map.

Chromatic aberration calibration

As mentioned above, chromatic aberration manifests itself as a 'barrel' distortion of the red channel and a 'pincushion' distortion of the blue channel, relative to the green channel. We emphasize that the distortion due to chromatic aberration is relative to the green channel. There is also an overall distortion effect across all channels; however, this is negligible when compared with the elasticity of skin. The effect of chromatic aberration can be seen in Fig. 3. Figure

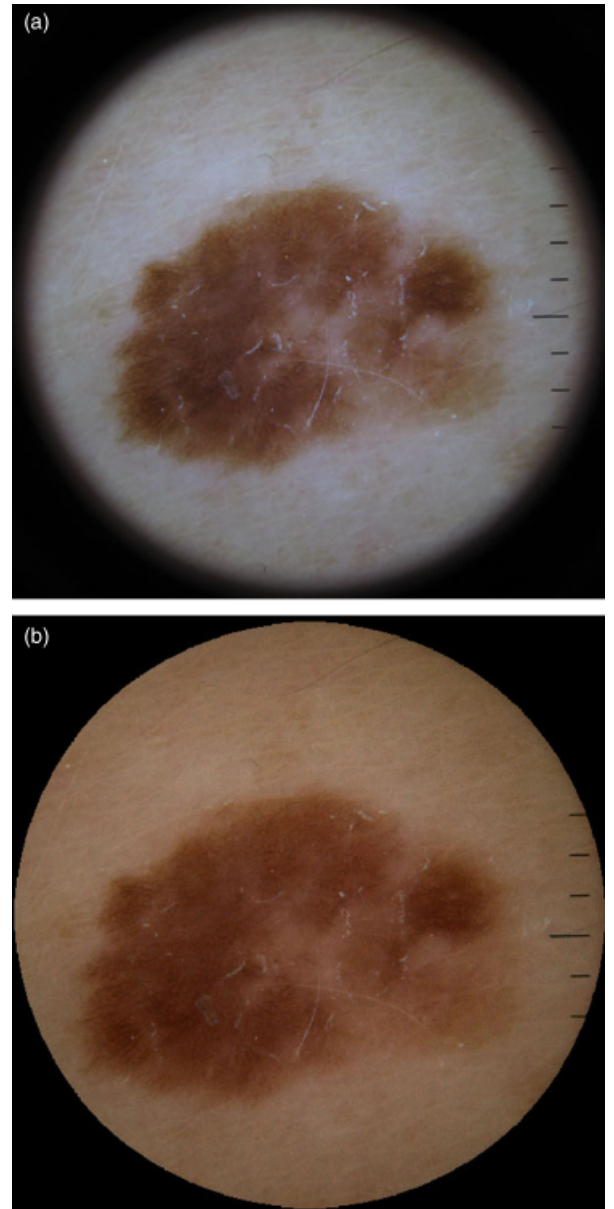


Fig. 2. Dermoscopic image of a melanoma in situ acquired with the Canon system as processed by (a) Canon's ZOOMBROWSER EX software (b) our color calibration procedure.

3b shows a magnified view of the upper left area, where the edge of the checkered pattern has a bluish tint along the upper and left edges and a reddish tint on the right and lower edges. This tinting is reversed in Fig. 3c, where the magnified view has a different location relative to the center of the lens.

Chromatic aberration is a form of radial distortion and thus has the following properties: (1) It is symmetric with respect to the center of the lens, (2) the magnitude of the distortion is a function of the distance to the center of the lens and (3) the direction of

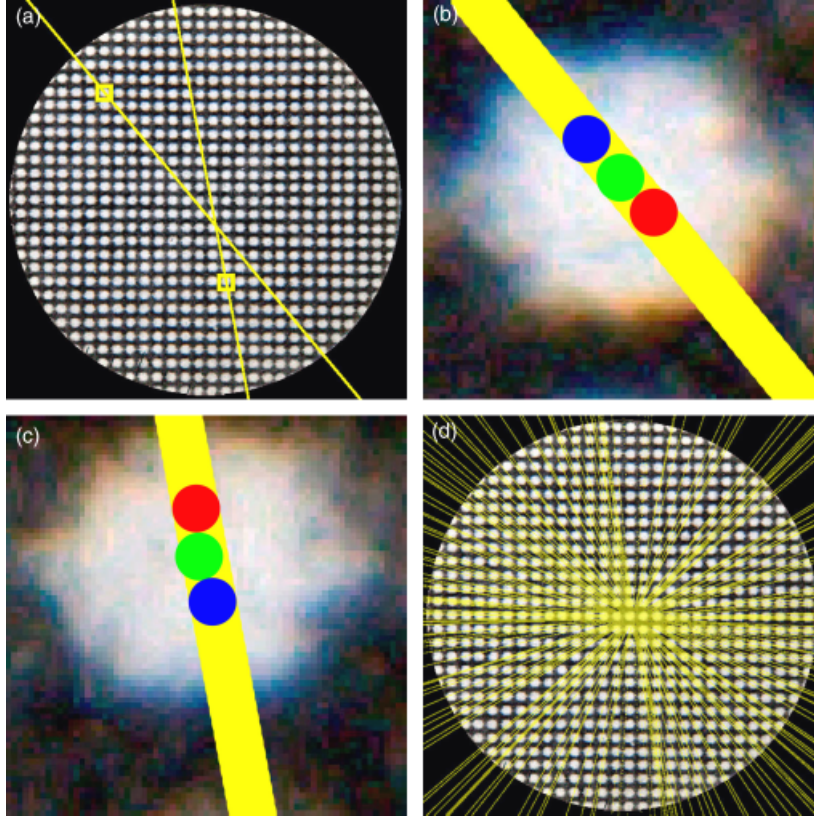


Fig. 3. Correcting for chromatic aberration. (a) The checkered pattern imaged with the dermoscope. The center of the lens can be found using lines that characterize the direction of distortion. (b) Magnified view of the upper left area; note the blue tint along the top and left edges of the squares and the red tint along the bottom/right. The centroids of each square in each channel are denoted by red, green and blue circles, respectively (distances between centroids have been exaggerated for illustrative purposes). These centroids are used to generate the yellow lines. (c) Magnified view of the lower right area; here the tinting is reversed due to the location of the squares with respect to the center of the lens. (d) Finding the center of the lens in image coordinates via least squares using many lines.

the distortion for any given point is radial, that is, along the line joining it to the center of the lens. We can therefore correct chromatic aberration by using a radial distortion model (9) once we have determined (1) the center of the lens in image coordinates and (2) the relationship between the magnitude of the distortion and the distance to the lens center. Both tasks can be accomplished by imaging a black and white checkered pattern.

Determining the center of the lens

The center of the lens is determined by examining the direction of the distortion in each square of the checkered pattern. The direction of the distortion in each square is characterized by a line. As the distortion is radial in nature, this line must also pass through the center of lens. We begin by computing the centroid of each square to sub-pixel accuracy in the red, green

and blue channels, respectively (as in Fig. 3b and c). These three points are used to define a line in the form $ax+by+c=0$. The center of the lens can be determined using two such lines (as in Fig. 3a); however, greater accuracy is achieved using the least squared solution to the intersection of multiple lines (as in Fig. 3d). Let (a_i, b_i, c_i) ; $i = 1, \dots, N$ represent the coefficients of the i th line computed from the i th square. The center of the lens (x_c, y_c) is the point that minimizes the sum squared distance to the lines as follows:

$$(x_c, y_c) = \operatorname{argmin}_{x,y} \sum_{i=1}^N d_i(x, y)^2$$

where $d_i(x, y)$ is the perpendicular distance from the point (x, y) to the i th line (a_i, b_i, c_i) :

$$d_i(x, y) = \frac{|a_i x + b_i y + c_i|}{\sqrt{a_i^2 + b_i^2}}$$

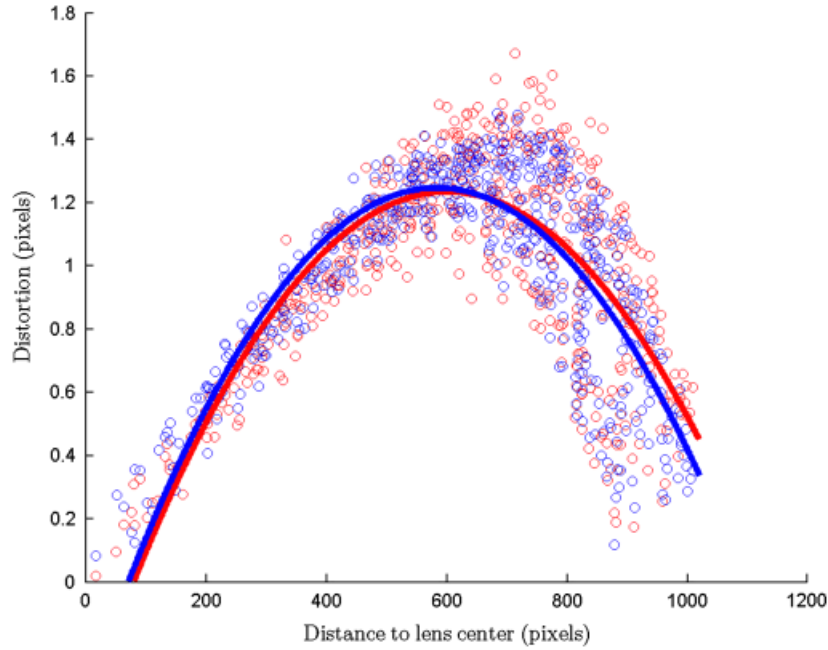


Fig. 4. Characterizing the distortion due to chromatic aberration with respect to the distance from the center of the lens in the red and blue channels. Each point represents the distortion at the center of a square of the checkered image while the lines represent the estimated distortion models of the system.

for which the closed-form solution is derived:

$$y_c = \frac{\sum_{i=1}^N b_i c_i \sum_{i=1}^N a_i^2 - \sum_{i=1}^N a_i c_i \sum_{i=1}^N a_i b_i}{\left(\sum_{i=1}^N a_i b_i\right)^2 - \sum_{i=1}^N b_i^2 \sum_{i=1}^N a_i^2}$$

$$x_c = \frac{-y_c \sum_{i=1}^N a_i b_i - \sum_{i=1}^N a_i c_i}{\sum_{i=1}^N a_i^2}$$

Determining the magnitude of the distortion

After determining the center of the lens, we use a second-order radial distortion model (8) to estimate the distortion of the red and blue channels. We seek to determine the function $D(r)$ that represents the distortion (measured in pixels) with respect to the distance from the lens center (also measured in pixels). We determine these distortion functions for the red [$D_R(r)$] and blue [$D_B(r)$] channels independently.

Red channel distortion $D_R(r)$ is sampled at each square of the checkered pattern by taking the distance between the red and the green centroids. The distance from the lens center (r) is measured with respect to the green centroid. Distortion in the blue channel is similarly obtained. After sampling these distortion functions at each square, the functions are modelled as second-order polynomials (illustrated in Fig. 4) to create a distortion map. The resulting polynomials are used to warp the red and blue channels to align

them with the green channel. The warping is performed as follows: for each pixel in the red and blue channels, a displacement vector is calculated. The magnitude of the vector is determined by $D(r)$ while the direction is set to be radial.

Results

We evaluate the effectiveness of our calibration procedure using our primary skin lesion imaging system (the ‘Canon system’) as well as a secondary system (the ‘Sony system’). The Sony camera is unable to acquire images in the ‘raw’ mode and therefore a method to perform white balancing must be specified. Custom white balancing was used so that the resulting transformation would be constant across images. The white patch of the color chart was used as reference white.

Color/lighting

To evaluate the effectiveness of color calibration, we follow the lead in (3) and report precision and accuracy values. Precision is the degree to which repeated measurements are reproducible, while accuracy is the degree to which measurements match those of a reference system (in this case, a spectrometer). Both are measured as ΔE , which represents Euclidian distances in the $L^*a^*b^*$ space, as $\Delta E = 1$ corresponds (approximately) to a just noticeable perceptual difference. As in (3), we

TABLE 1. Precision and accuracy measurements for both imaging systems compared to previous work

	Precision		Accuracy	
	Mean	Maximum	Mean	Maximum
Canon system	6.4	14.8	0.43	1.2
Sony system	10.0	23.6	10.2	22.4
Vander Haeghen et al. (3)	6.2	13.3	0.30	1.2

report the mean and maximum values. Table 1 summarizes the results.

Chromatic aberration

To analyze the effect of chromatic aberration correction, we consider the joint distribution of the pixels' red and blue intensity values in the checkered image. Under ideal conditions, we would expect to see only two types of pixels: black and white. If we were to plot such a joint distribution, we would expect to see two distinct regions: the first at the bottom left representing the black pixels and the second at the upper right representing the white pixels. However, due to the limitations in the resolution of the camera (as well as in the chequered pattern itself), we observe many partial volume effects along the black/white borders, resulting in the inclusion of various shades of gray pixels. Consequently, we would expect such a joint distribution to include a region along the line joining the ideal black and white pixels. Chromatic aberration further distorts this distribution by conferring red and blue hues to these gray edge pixels, creating a 'bulge' in our idealized line distribution.

We can therefore visually evaluate the effect of chromatic aberration correction by examining these joint distributions. Figure 5 shows such distributions before and after correcting for chromatic aberration in the Canon system. The effect can also be quantified by taking the moment of inertia of the distribution about the idealized line distribution. This is equivalent to measuring the sum squared distance of the pixels from the idealized line (where distance is Euclidian rather than the vertical). For a frequency distribution $F(r, b)$, the moment is calculated as follows:

$$I = \sum_{r=0}^{255} \sum_{b=0}^{255} \frac{F(r, b)(r - b)^2}{2}$$

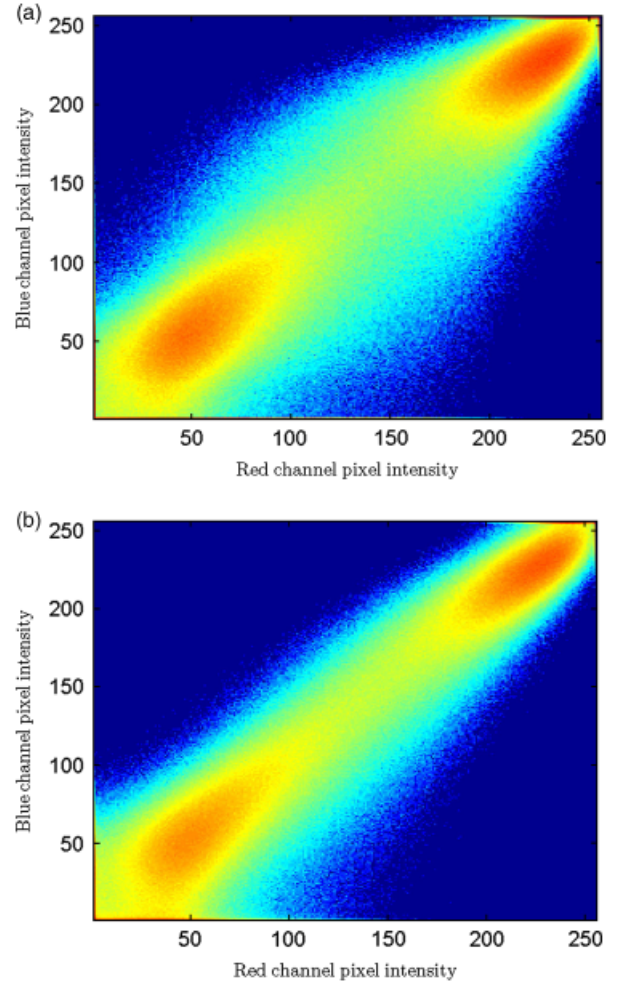


Fig. 5. Log-frequency plots of the joint distribution of pixel intensities (red channel vs. the blue channel) for the checkered image as imaged by the Canon system (a) before correcting for chromatic aberration and (b) after. As the checkered image is grayscale, all the pixels would fall on the diagonal line under an ideal imaging system. The log of the frequencies was plotted for visualization purposes.

For the Canon system, the moment before and after correction is 562.8 and 296.9, respectively, resulting in an improvement of 47.2%. For the Sony system, the moments are 442.8 and 258.1, respectively, resulting in an improvement of 41.7%. The effect of chromatic aberration correction on the checkered pattern in the Canon system is shown in Fig. 6.

Discussion

As can be seen in Table 1, the accuracy and precision values for the Canon system closely match those of the previous work, while the Sony system fares considerably worse. It is believed that this difference can be attributed to the inability to access the raw sensor data on the Sony camera. There are many proprietary trans-

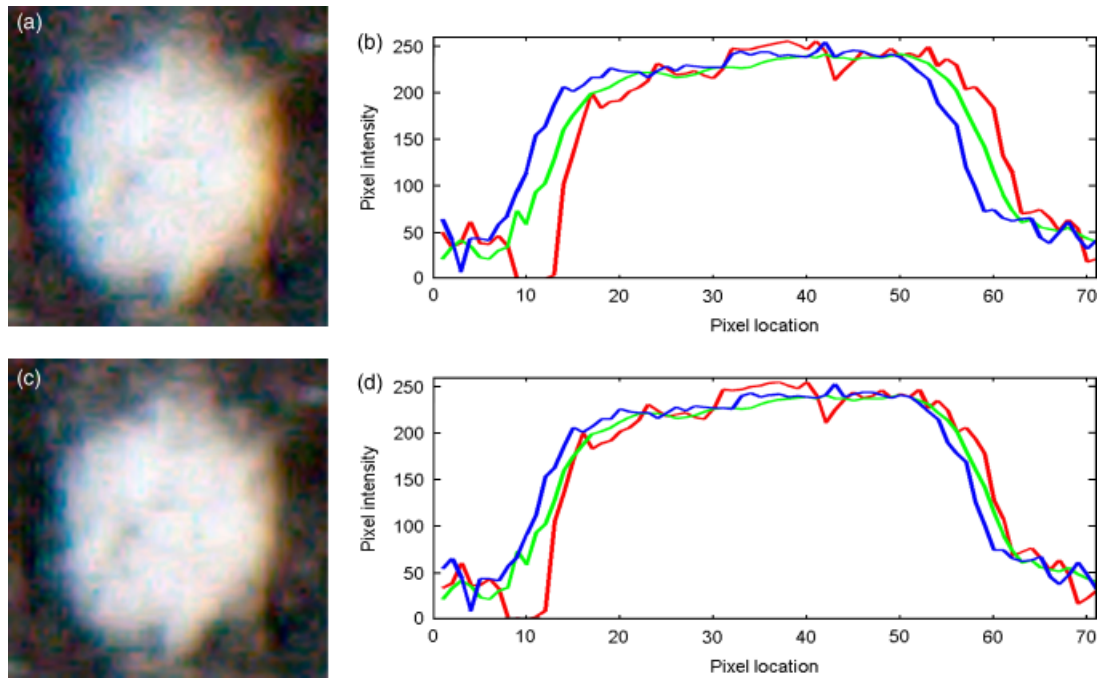


Fig. 6. The effects of chromatic aberration correction on the checkered pattern as imaged by the Canon system (a, b), before chromatic aberration correction and (c, d) after chromatic aberration correction. Notice the reduction in the red and blue halos as well as the alignment of the edges in the intensity plots.

formations that consumer cameras perform on raw sensor data in the name of esthetics when converting to a standard image format such as tiff or jpeg. If these transformations are constant across images, then under certain conditions, it is possible that calibration can undo them. If, however, these transformations are not constant across images (e.g. contrast normalization), then it is impossible for a calibration method to correct for this. It is suspected that the relatively poor precision and accuracy observed in the Sony system is due to such transformations. This gives strong motivation for ensuring that a camera has raw mode capabilities if it is to be used in a setting where accurate color reproduction is important.

Chromatic aberration is an interesting phenomenon that has hitherto gone unstudied in

digital dermoscopy. While expensive optical systems are designed to mitigate chromatic aberration optically, the growing tendency to create low-cost ad hoc digital dermoscopes suggests that this will only become more of a concern in the future. As chromatic aberration can be partially managed via camera settings, we recommend always using the minimum aperture size with any digital dermoscope that uses a consumer-grade camera. Additionally, we show that chromatic aberration can be further mitigated via software-based calibration.

Furthermore, it may be possible to exploit chromatic aberration for beneficial ends, such as improving the automatic detection of hair in dermoscopic images (10).

References

1. Perednia DA, Brown NA. Teledermatology: one application of telemedicine. *Bull Med Libr Assoc* 1995; 83: 42–47.
2. Day GR, Barbour RH. Automated melanoma diagnosis: where are we at? *Skin Res Technol* 2000; 6: 1–5.
3. Vander Haeghen Y, Naeyaert JM, Lemahieu I, Philips W. An imaging system with calibrated color image acquisition for use in dermatology. *IEEE Trans Med Imaging* 2000; 19: 722–730.
4. Grana C, Pellacani G, Seidenari S. Practical color calibration for dermoscopy, applied to a digital epiluminescence microscope. *Skin Res Technol* 2005; 11: 242–247.
5. Maglogiannis I. Design and implementation of a calibrated store and forward imaging system for teleder-

- matology. *J Med Syst* 2004; 28: 455–467.
6. Spaces C. Consistent cutaneous imaging with commercial digital cameras. *Arch Dermatol* 2006; 142: 42–46.
 7. Coffin D. Dcraw software. 2008. Available at <http://www.cybercom.net/~dcoffin/dcraw/> (accessed March 23, 2010).
 8. Ebner M. *Color constancy*. New York: Wiley, 2007.
 9. Devernay F, Faugeras O. Automatic calibration and removal of distortion from scenes of structured environments. *Proc Soc Proc Inst Eng* 1995; 2567: 62–72.
 10. Wighton P, Lee TK, Atkins MS. Dermoscopic hair disocclusion using inpainting. *Proc Soc Proc Inst Eng* 2008; 6914: 691427–6914278.

Address:
Tim K. Lee
Cancer Control Research and Cancer Imaging
BC Cancer Agency
675 West 10th Avenue
Vancouver, BC
Canada V5Z 1L3
e-mail: tlee@bccrc.ca